DNA methylome and transcriptome alterations in high glucose-induced diabetic nephropathy cellular model and identification of novel targets for treatment by Tanshinone IIA

Journal:	*Chemical Research in Toxicology*
Manuscript ID	tx-2019-00117k.R1
Manuscript Type:	Article
Date Submitted by the Author:	n/a
Complete List of Authors:	Li, Wenji; Yangzhou University; Rutgers The State University of New Jersey Sargsyan, Davit; Rutgers The State University of New Jersey Wu, RenYi; Rutgers University Ernest Mario School of Pharmacy, Pharmaceutical Sciences li, Shanyi; Rutgers The State University of New Jersey Wang, Lujing; Rutgers The State University of New Jersey Cheng, David; Rutgers University Ernest Mario School of Pharmacy, Pharmaceutical Sciences Kong, Ah-Ng; Rutgers University - SUNJ, Department of Pharmaceutics, Center for Cancer Prevention Research

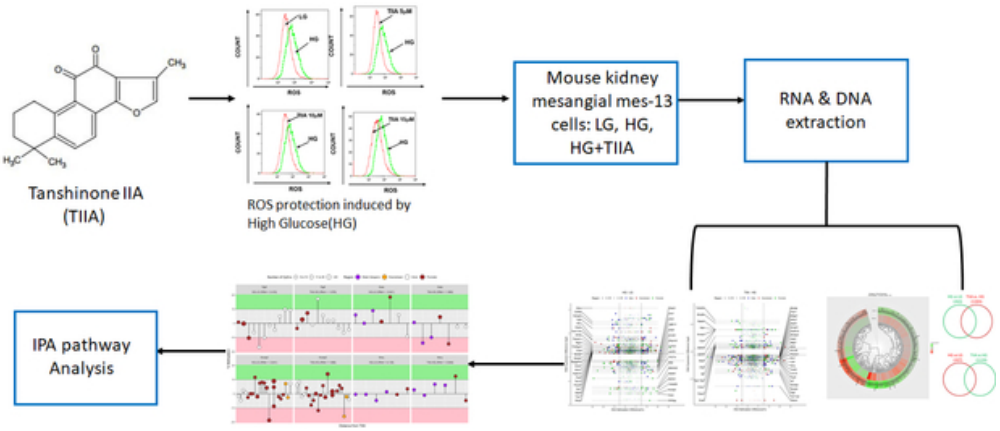

Graphic Abstract

26x11mm (600 x 600 DPI)

DNA methylome and transcriptome alterations in high glucose-induced diabetic nephropathy cellular model and identification of novel targets for treatment by Tanshinone IIA

Wenji Li [a,b,c,#], Davit Sargsyan[c,d,e,#], Renyi Wu[c,d], Shanyi Li[c,d], Lujing Wang[c,d,e], David Cheng[c,d,e] and Ah-Ng Kong[c,d,*]

[a,] Institute of Translational Medicine, Medical College, Yangzhou University, Yangzhou, 225001, PR China

[b,] Jiangsu Key laboratory of integrated traditional Chinese and Western Medicine for prevention and treatment of Senile Diseases, Yangzhou University, Yangzhou, 225001, PR China

[c,] Department of Pharmaceutics, Ernest Mario School of Pharmacy, Rutgers, The State University of New Jersey, 160 Frelinghuysen Road, Piscataway, NJ 08854, USA

[d,] Center for Phytochemical Epigenome Studies, Ernest Mario School of Pharmacy, The State University of New Jersey, Piscataway, NJ 08854, USA.

[e,] Graduate Program in Pharmaceutical Sciences, Ernest Mario School of Pharmacy, The State University of New Jersey, Piscataway, NJ 08854, USA.

[#]equal contribution

Correspondence should be addressed to:

* Professor Ah-Ng Tony Kong, Department of Pharmaceutics, Ernest Mario School of Pharmacy, Rutgers, The State University of New Jersey, 160 Frelinghuysen Road, Piscataway, New Jersey 08854, Phone: 732-455-3831; Fax:732-455-3134; E-mail: KongT@pharmacy.rutgers.edu

Date: May 7th, 2019

Abstract

Diabetic nephropathy (DN) is a diabetes complication which comes from overactivation of Renin-Angiotensin System, excessive proinflammatory factors, reactive oxygen species (ROS) overproduction, and epigenetic changes. Tanshinone IIA (TIIA), a diterpene quinone phytochemical has been shown to possess powerful antioxidant, anti-inflammatory, epigenetics and protective effects against different diseases including DN by inhibiting ROS induced by high glucose (HG). However, epigenomic and transcriptomic study of DN and the protective effect of TIIA are lacking. In this study, next-generation sequencing (NGS) of RNA and DNA methylation profiles on the potential underlying mechanisms of a DN model of mouse kidney mesangial mes13 cells challenged with HG and treatment with TIIA were conducted. Bioinformatic analysis coupled with Ingenuity Pathway analysis (IPA) of RNAseq were performed and 1,780 genes from HG/LG and 1,416 genes from TIIA/HG were significantly altered. Several pro-inflammatory pathways like leukotriene biosynthesis and eicosanoid signaling pathways were activated by HG stimulation while TIIA treatment would enhance glutathione-mediated detoxification pathway to overcome the excess oxidative stress and inflammation triggered by HG. Combination analysis of RNA-seq and Methyl-seq datasets, DNA methylation and RNA expression of a list of DN associated genes, *Nmu, Fgl2, Glo, and Kcnip2* were found to be altered in HG-induced mes13 DN model, and TIIA treatment would effectively restore the alterations. Taken together, these findings provide novel insights into the understanding of how epigenetic modifications could affect the progression of DN and the potential preventive effect of TIIA in DN.

Key Words: Diabetic nephropathy, Tanshinone IIA, IPA, methyl-seq, RNA-seq

1. Introduction

Diabetic nephropathy (DN) manifested glomerular hyperfiltration and proteinuria in function, and renal hypertrophy, basement membrane thickening, extracellular matrix(ECM) accumulation, glomerulosclerosis, and interstitial fibrosis in histology, and finally developed into renal failure.[1] Pathological factors attributes to development of DN were acknowledged to be a complexation of overactivation of Renin-Angiotensin System, excessive proinflammatory factors, reactive oxygen species (ROS) overproduction, and epigenetic changes.[2-4]

Among them, ROS overproduction played an important role in inducing apoptosis and kidney cell damage upon high glucose (HG) stimulations. [5, 6] Multiple kidney cells were found to generate excessive ROS by stimulation of high glucose.[7, 8] Overexpression of proinflammatory factors, such as transforming growth factor-β1 (TGF-β1), has proved to be highly associated with ECM accumulation and glomerulosclerosis.[9] Overactivation of TGF-β1 would induce excessive ROS, which will in turn enhance the level of TGF-β1 and worsen the condition of DN.[10]

Nuclear factor erythroid 2-related factor 2 (Nrf2), one of the most important cellular defense mechanisms with the ability to modulate many phase II detoxifying enzymes by binding to ARE (antioxidant response element) of those genes and maintain cellular redox hemeostasis,[11] has shown to be vital in regulating the antioxidative stress response and is essential for the anti-inflammatory response in many clinical and preclinical studies.[12] Accumulating data suggest that many dietary phytochemicals can induce Nrf2-mediated antioxidant/anti-inflammatory signaling pathways.[13] Hence many of them are used for inhibiting DN.[14-16]

Tanshinone IIA (TIIA), a diterpene quinone phytochemical isolated from Salvia miltiorrhiza has a long history of application for cardiovascular disease.[17] Notably, TIIA can suppress reactive oxygen species (ROS) and inflammation through activating Nrf2 pathway.[18, 19] Besides cardioprotective effect, TIIA also possesses multiple pharmacological effects, including antioxidant,[20] anti- angiogenesis,[21] anti-inflammatory[22] and neuroprotective effects,[23] which contributes to its diverse therapeutic spectrum including diabetes.[24, 25] TIIA exhibits protective effects on both acute kidney injury[26, 27] and chronic renal disorders.[28, 29]

However, there are very limited evidences of TIIA on DN, which all used rat cells or streptozotocin (STZ) induced type I DN rat model.[24, 30, 31] In addition, the underlying mechanism of action is not clear. A systematic screening for targets of TIIA effects on DN is highly needed.

More and more emerging evidences indicates Epigenetic changes, including DNA methylation, histone post-translational modifications (PTMs), and noncoding RNA-mediated post-transcriptional alterations, are closely related to DN.[32-34] Next-generation sequencing (NGS) on whole genome or epigenome would provide systematic means in analyzing new biomarkers associated with DN which will provide a novel target for treatment. NGS results including RNA-seq and non-coding RNA-seq began to reveal the novel DN associated biomarkers genome wide.[35, 36] However, there lacks whole DNA methylome especially whole methylome and transcriptome synergistically investigations into the pathological changes of DN. This paper will report our work on DNA methyl-seq and mRNA-seq co-alterations using a high-glucose induced mouse kidney mesangial cell model which represents diabetes in vitro. The NGS results comparison between high glucose, low glucose and TIIA will also provide identification of novel targets for diabetic nephropathy and treatment by TIIA.

2. Material & Methods

2.1 Materials

Dulbecco's modified Eagle's medium, fetal bovine serum (FBS), penicillin-streptomycin (10,000 U/ml), puromycin, versene, and trypsin-EDTA were supplied by Gibco (Grand Island, NY, USA). TIIA and dimethyl sulfoxide (DMSO) were purchased from Sigma-Aldrich (St. Louis, MO, USA).

2.2 Methods

2.2.1 Mouse mesangial cell culture

SV40 MES 13 mouse kidney mesangial cells were obtained from the American Type Culture Collection (Manassas, VA, USA) and maintained in Dulbecco's modified Eagle's medium (Gibco; Thermo Fisher Scientific, Inc.) with 14 mM HEPES (Gibco; Thermo Fisher Scientific, Inc.) and 5% FBS (Gibco; Thermo Fisher Scientific, Inc.) at 37°C with 5% CO2. Mesangial cells were seeded at 1×10^5 cells/10 cm dish and were treated with serum free medium for 1 day followed by 0.1%DMSO in 30 mM D-glucose (high glucose, HG) or 0.1%DMSO in 5.5 mM D-glucose + 24.5 mM D-mannitol (isotonic control, low glucose, LG), or TIIA (5μM,10 μM, 15 μM dissolved in 0.1%DMSO in low glucose) for 5 days.

2.2.2 Intracellular ROS detection

CM-H2DCFDA (Invitrogen) was used as the probe. Mes-13 cells were treated with 0.1% DMSO in LG, 0.1%DMSO in HG or TIIA (5μM,10 μM, 15 μM in 0.1% DMSO in HG) for 48 h. The cells were grown to 90% confluence, washed with PBS and then harvested using trypsinization, according to the manufacturer's protocol. The cells were then washed four times and incubated with 10 μM CM-H2DCFDA for 45 min at 37°C in a relatively high humidity (95%) atmosphere containing a controlled level of CO_2 (5%) in the dark. Finally, cell-associated mean fluorescent intensity was measured by flow cytometry in FL1 channel excitation and emission wavelengths were 488 and 525 nm, respectively.

2.2.3 Total RNA/DNA extraction, library preparation, RNA-seq and methyl-seq

Total RNA and DNA was extracted from SV40 MES 13 mouse kidney mesangial cells from LG, HG and TIIA groups using the AllPrep DNA/RNA Mini Kit (Qiagen, Valencia, CA, USA). The quality and quantity of the extracted RNA and DNA samples were determined with an Agilent 2100 Bioanalyzer and NanoDrop, respectively. A total of 3 RNA and DNA pooled samples from each group were sent to RUCDR for library preparation and sequencing. Briefly, the library of RNA-seq was constructed using the Illumina TruSeq RNA preparation kit (Illumina, San Diego, CA, USA) according to the manufacturer's manual. Samples were sequenced on the Illumina NextSeq 500 instrument with 50–75 bp paired-end reads, to a minimum depth of 30 million reads per sample. The DNA samples were further processed using an Agilent Mouse SureSelect Methyl-seq Target Enrichment System (Agilent Technologies, Santa Clara, CA) and sequenced on an Illumina NextSeq 500 instrument with 76-bp single-end reads, generating 34–47 million reads per sample.

2.2.4 Data Analysis

Sequencing data quality was checked using FastQC 0.11.2 software.[37] Linux-base bioinformatics software packages SAMtools (Sequencing Alignment/Map tools)[38] and HIDSAT-2 (hierarchical indexing for spliced alignment of transcripts)[39] were used to sort, deduplicated, index and align reads in RNA sequencing files. DNA methylation data was processed with Bismark tool.[40] All reads were aligned to the mouse reference genome (mm9.2) R 3.5.1 (R Core Team)[41] was used for all downstream statistical analysis and visualization of RNA and DNA sequencing data.

2.2.5 Differential Gene Expression Analysis

Total of 24,421 genes were mapped. Genes with low counts (less than 20 counts in all samples combined) were removed from the analysis. The remaining 13,954 genes were further examined. Two comparisons - high glucose(HG) vs. low glucose (LG), and TIIA in HG vs HG only, were done using an R package

DEGSeq [42] to identify differentially expressed genes. The genes with the log2 difference of at least 0.3 and filtered by q-values as defined by Storey et al[43] were selected. The MA plots (log differences vs log means) for the two comparisons are shown in the Figure 1. The RNA expression patterns of the selected genes were further explored to isolate genes that were affected by the HG treatment but restored by the TIIA.

2.2.6 SureSelect Methyl-seq analysis

After alignment, DMRfinder (version 0.1) was used to extract methylation counts and cluster CpG sites into DMRs.[44] Each DMR was defined to contain at least three CpG sites. Genomic annotation was performed with ChIPseeker (version 1.10.3) in R.[45] To examine the associations of DNA methylation and the downstream RNA expression, the differences in percent methylation and RNA expressions for the genes selected in the RNA-seq analysis were plotted against each other. The genes that exhibited DNA hypermethylation in promoter and RNA downregulation, or DNA hypomethylation in promoter and RNA upregulation, were selected as genes of interest for further analysis.

2.2.7 Ingenuity Pathway Analysis (IPA) Analysis

Isoforms with $\log_2$ ratios greater than 0.3 or less than -0.3 and filtered by q-values were subjected to Ingenuity Pathway Analysis (IPA 4.0, Ingenuity Systems, www.Ingenuity.com). The input isoforms were mapped to IPA's database, and the top related genes, relevant biological functions, diseases and canonical pathways related to HG induced pathological changes and TIIA interventions were identified.

2.2.8 Quantitative polymerase chain reaction (qPCR) validation of genes of interest

qPCR was used to validate the expression trends of selected genes of interest identified by methyl-seq and RNA-seq. First-strand cDNA from isolated 300 ng mRNA from pooled samples was synthesized using TaqMan® Reverse Transcription reagents (Applied Biosystems, Carlsbad, CA, USA). qPCR was carried out using a QuantStudio™ 5 Real-Time PCR System (Applied Biosystems) with SYBR Green PCR

Master Mix (Applied Biosystems) with the qPCR primers listed in Table 1. The gene expression fold changes were normalized to the expression of beta-actin using the 2^−ΔΔCT method (RQ values). The gene expressions from HG group were normalized to 1 and the relative fold changes were obtained from the comparation between the other 2 groups to HG group. All the primers were designed and ordered from Integrated DNA Technologies (IDT, Coralville, Iowa, USA).

2.2.9 Statistical analysis

The data are presented as the mean ± standard deviation (std). One-way analysis of variance (ANOVA) test was performed to test for the differences between the mean RQ values of the three treatment groups, followed by a post hoc pairwise comparisons (Dunnett's test). Differences with p-values less than 0.05 were considered statistically significant.

3. Results

TIIA exerted protection effect on intracellular reactive oxygen species (ROS) induced by high glucose

In mouse kidney mes-13 cells, 2 days treatment of high glucose (HG) will induce 1-fold increase of intracellular ROS damage comparing with low glucose group (Figures 2A&E), while co-treatment of TIIA (5μM, 10 μM and 15 μM) (Figures 2B, C, D &E) could protect mes-13 cells against ROS damage by HG. Excessive ROS is highly associated with apoptosis and kidney cell damage upon HG stimulations in DN [5, 6] and TIIA treatment has shown a very promising reversal efficacy especially at 5 μM concentration. Hence, in the following NGS study, we treated mes-13 cells at this concentration for 5 days to study the global epigenomics change induced by TIIA in preventing DN.

Global transcriptome results comparison

Global gene expressions were ranked in the order of expression $\log_2$ fold change. 1,780 genes from HG/LG and 1,416 genes from TIIA/HG with the $\log_2$ fold change levels of 0.3 or more (both, positive and negative) were then used as an input to the IPA software. Top 50 annotated genes with the highest log2-

fold change in either direction in HG over LG comparison and top 50 annotated genes with the highest log2-fold change in either direction in TIIA over HG were listed in Table 2 and 3 respectively. Doughnut Heatmap (Figure 3A) demonstrates the 213 overlapping genes with $\log_2$ fold changes greater than 0.3 and filtered by q-values which show reversal of the effect of HG treatment by TIIA. The detailed 213 differentially expressed genes in HG/LG and TIIA/HG comparisons are listed in Supplement Table 1. As indicated in the Venn diagrams, there are 263 genes increased in HG versus LG and 1,393 genes decreased in TIIA versus HG. Among them, same 124 genes both increased in HG over LG and decreased in TIIA over HG (Figure 3B). There are 207 genes decreased in HG over LG and 1,120 genes increased in TIIA over HG. Among them, same 89 genes both decreased in HG over LG and increased in TIIA over HG (Figure 3C). Those 124 overlapping genes from HG/LG and 89 from TIIA/HG which show the opposite trends in the comparisons were marked as candidates for the genes of interest.

SureSelect Methyl-seq analysis

To understand the involvement of DNA methylation in DN, we determined the single-base-resolution DNA methylation of mouse kidney mesangial cells from LG, HG and TIIA groups. A comparison of the methylation landscape across the treatments showed that overall methylation levels differed by the region but not by treatment, e.g. methylation ratios were much lower in the promoter regions compared to body and intergenic (downstream) regions (Figure 4a). Majority of DMRs consisted of a small number of CpGs (3 to 7) (Figure 4b), with nearly a quarter of CpG located in the promoter region (Figure 4c).

Correlation of SureSelect Methyl-seq results with RNA-seq results

Mounting evidences have suggested that the methylation status alteration of gene promoters, unlike other regions, caused reversed gene expression change: hypermethylation of coding or noncoding gene promoters correlates with the reduced expression of them and hypomethylation correlates with increased expression.[46] Based on this notion, we prepared starburst figures to show the association between DNA methylation and gene expression of the 213 overlapping genes from the RNA-seq results (Figures 5a and

5b). The genes with green dots (corresponding to promoters) in the upper left and the lower right quadrants suggested reversed alteration of methylation in promoters with RNA expression levels. DNA methylation level differences of these genes along with the gene expression differences are presented as Lollipop plots (Figure 7).

Validation of selected gene expression which shows close correlation between RNA-seq and methyl-seq by quantitative real-time RT-PCR

Genes of interest expression in HG were normalized to 1. In Figure 6, relative expression of *Gulo* and *Kcnip* were significantly decreased from 1.65 to 1 and 1.29 to 1 in comparing LG with HG and increased from 1 to 1.54 and 1 to 1.20 from HG to TIIA respectively ($p<0.05$). Relative expression of *Fgl2* were significantly increased from 0.67 to 1 from LG group to HG group and decreased from 1 to 0.74 from HG to TIIA ($p<0.05$). The relative expression of *Nmu* were increased from 0.80 to 1 (from LG to HG) and decreased from 1 to 0.84 (from HG to TIIA). All these change trend correlates well with the RNA-seq results (Table 4).

Lollipop figures show the association between SureSelect methyl-seq and RNA-seq results

The Lollipop plots (Figures 7A,B,C,D,E,F,G,H) provides in-depth understanding of RNA expression and DNA methylation difference within the HG/LG and TIIA/HG comparisons. The length of the stem corresponds to the methylation ratio, up or down orientation indicates the increase or decrease of methylation, and the color of the bubble codes for the different methylation regions (distal intergenic region: purple; downstream: yellow; intron: white; promoter: red). RNA expression of genes of interest are also listed in the figure. The Lollipops figures are in good accordance with SureSelect methyl-seq results and demonstrate the association between DNA promoter methylation ratio and RNA expression. *Fgl2 and Nmu* indicate a methylation ratio decrease in promoter region in HG/LG and the ratio increase in TIIA/HG. In addition, the genes expression from RNA-seq shows an increase in HG/LG and decrease in TIIA/HG. *Gulo and Kcnip2* have opposite changes in DNA promoter methylation ratio and gene

expression with Fgl2 and Nmu. These results suggest treatment of TIIA can reverse HG influence in DNA promoter methylation and gene expression in the 4 genes of interest.

Discussions

Top differentially canonical pathways, Tox and diseases influenced by HG and treatment by TIIA identified by IPA analysis

Figure 8 indicates the 10 most significant associated canonical pathways identified by IPA from all significant and reliable Differentially expressed genes in HG versus LG (Figure 8a) and TIIA versus HG groups (Figure 8b) from mes-13 cells after 5 days treatment. In the top 2 significant associated pathways in the comparison group of HG versus LG, HG can induce both Leukotriene biosynthesis and Eicosanoid Signaling, which are both highly related to enhance proinflammation factors like leukotrienes, prostaglandin, cyclooxygenases (COX-1 and COX-2), promote inflammation and amplify immune response. Leukotrienes are proinflammatory metabolites of arachidonic acid(AA) that activate and amplify innate and adaptive immune responses.[47] They can induce leukocyte aggregation, activate phagocyte and generate proinflammatory factors.[48] Four major types of eicosanoids, prostaglandins, lipoxins, leukotrienes and thromboxanes are generated by AA through Prostaglandin endoperoxide synthases or lipoxygenases.[49] Eicosanoids can modulate complicated oxidative response, inflammation, allergy and carcinogenesis.[50] Our in vitro long-term HG treatment seems to be able to enhance oxidative stress and inflammation response in mouse kidney mesangial cells mainly via Leukotriene biosynthesis and Eicosanoid Signaling pathway.

In the top 2 significant associated pathways in the comparison group of TIIA versus HG, TIIA can influence Liver X receptor (LXR)/ The retinoid X receptors (RXR) activation and enhance glutathione-mediated Detoxification. LXR/ RXR has a close relation with the regulation of metabolism of glucose, lipid and cholesterol and inflammation.[51] Tripeptide glutathione (GSH) forms thioether conjugates with leukotrienes, prostaglandin and other chemicals, which can be subsequently degraded by Gamma-

glutamyl hydrolase or γ-glutamyl transpeptidase, and dipeptidases.[52] Our findings suggest TIIA treatment can restore the cellular response induced by HG mainly targeting the above two pathways.

The Tox Analysis by IPA is to indicate most associated biological processes and toxicological responses to xenobiotic influence. In the top 10 mostly associated tox changes (Figure 9), majority toxicological response in HG/LG and TIIA/HG are both mainly associated with kidney disorders, which suggest the suitability of High glucose induced mes-13 cell model as an in vitro DN cell model. In Figure 10, the most associated disease types, both HG/LG and TIIA/HG models are highly associated with endocrine system disorders and organism injuries, which correlate well with DN.

Correlated genes of interest

Based on the analysis of sureselect-methy-seq and RNA-seq results, we identified 4 most relevant genes, in which HG can induce DN pathological associated changes in gene expression and accompanying with an opposite DNA methylation change in DNA promoter, while TIIA can restore the alteration to normal.

NMU, a neuropeptide belongs to the neuromedin family can generate active neuropeptides and regulate pain, stress, cancer and inflammatory diseases.[53] Recent findings indicate that NMU can act directly on pancreas β cells through NMUR1 in an autocrine or paracrine fashion to suppress insulin secretion.[54] In our in vitro system, HG can induce a very according high *Nmu* expression fold change (17.495) over LG, which is the highest fold change in HG/LG comparison (Table 4) accompanying with a decrease in DNA methylation (-0.526) of *Nmu* promoter, which suggest increase of *Nmu* by HG correlates with the decrease of DNA methylation in its promoter region. TIIA can reverse the change in gene expression and DNA methylation and indicating the potential therapeutic target on *Nmu*. Fibrinogen-like protein 2 (FGL2) is a novel prothrombinase. Increased *Fgl2* level was found to be highly correlated with the circulating TNF-α levels and severity of mouse type 2 diabetic nephropathy.[55] Like *Nmu*, HG can induce a very according high *Fgl2* expression fold change (5.346) over LG accompanying with a decrease in DNA

methylation (-10.324) of *Nmu* promoter. TIIA treatment also demonstrate a relative restoration effect on both gene expression and DNA methylation.

L-gulono-gamma-lactone oxidase (GLO), a necessary enzyme for ascorbic acid synthesis, was found to be decreased in diabetic rats.[56] In a Type 2 rat diabetes model, Potassium voltage-gated channel interacting protein 2 (KCNIP2/KChIP2) were found to be down-regulated.[57] Our results (Table 4) echoes the above findings that HG can decrease *Glo* and *Kcnip2* greatly (both 0.121) and correlates with an increase in the methylation ratio in their promoters (18.530 and 11.567 respectively). TIIA can effectively reverse the alteration in both gene expression and DNA methylation.

Those four genes of interest will be targets for our further investigation.

4. Conclusion

In conclusion, this study demonstrated the TIIA protective effect of against HG induced damage to kidney. Using SureSelect Methyl-seq and RNA-seq, we provided a quantitative global profile of the methylome and transcriptome in mouse kidney mesangial cells from LG and HG with or without TIIA treatment. IPA analysis identified inflammation pathways like Leukotriene biosynthesis and Eicosanoid Signaling were activated by HG stimulation while TIIA treatment may enhance glutathione-mediated Detoxification pathway to overcome the resulted excess oxidative stress and inflammation. Importantly, we identified that DNA methylation of a list of DN associated genes, *Nmu, Fgl2, Glo, and Kcnip2* were altered in HG induced DN model, and TIIA treatment effectively restored the DNA methylation and gene expression. These findings provide novel insights into the understanding of how epigenetic modifications affect the progression of DN and the preventive effect of TIIA.

Conflicts of interest

The authors declare that there are no conflicts of interest.

Acknowledgments

This work was supported in part by institutional funds and by R01-AT007065 from NCCIH and the Office of Dietary Supplements (ODS). The authors express sincere gratitude to all members of Dr. Tony Kong's laboratory for their helpful discussions.

Table and Figure Legends

Tables

Table 1. Real-time q-PCR Primers information of validated genes of interest

Table 2. Top 50 annotated genes showing the highest log_2-fold change in either direction in high glucose treated group (HG) over low glucose treated group (LG), ranked by log_2-fold change

Table 3. Top 50 annotated genes showing the highest log_2-fold change in either direction in 5μM TIIA treated group (TIIA) over HG, ranked by log_2-fold change

Table 4 Correlation of DNA promoter methylation ratio from SureSelect Methyl-seq and fold change of gene expression from RNA-seq for genes of interest

Figures

Figure 1. MA plots (log_2 means vs. log_2 difference) of the gene expressions in the two comparisons, HF vs. LG (A) and TIIA in HG vs. HG only (B). The two horizontal dotted lines correspond to log_2 differences of +/-0.3. The green or red symbols corresponds to upregulated or downregulated genes with FDR values of 0.5 or less

Figure 2. Effects of TIIA on production of intracellular reactive oxygen species (ROS) induced by 2 day treatment of high glucose (HG) In mouse kidney mes-13 cells via flow cytometry. Two days treatment of HG induced increase of intracellular ROS damage comparing with low glucose (LG) group(A), co-treatment of 5μM TIIA (B), 10 μM TIIA (C) and 15 μM TIIA(D) could protect mes-13 cells against ROS damage from HG. Relative ROS fold change normalized by LG (E) are expressed as means ± Std for 3 independent replicates and significant ($p<0.05$, *; $p<0.01$, **) difference comparing with HG are indicated.

Figure 3. Overview of the differentially expressed genes in 2 comparisons among 3 groups (HG/LG and TIIA/HG). (A) Doughnut Heat map of 213 overlapped Genes with differential expression that appeared in HG versus LG group and TIIA versus HG group. (B, C) Venn diagrams comparing the up-regulated (green) and down-regulated genes (red) between HG versus LG group and TIIA versus HG group. Genes with log2 fold changes greater than 0.3 were counted.

Figure 4. Sureselect Methyl-seq results (A) Percent of Methylated CpG by region and treatment; (B) Distribution of DMR by Number of CpG and Region; (C) DMR annotation by region (%)

Figure 5 Starburst figures indicating correlation between RNA-seq and methyl-seq. The upper left and lower right quadrantal region of indicate those genes with reversed change of methylation and RNA expression in HG/LG (A) and TIIA/HG(B) comparisons

Figure 6. RNA qPCR validation for the genes of interest. The gene expressions from HG group were normalized to 1 and the relative fold changes were obtained from the comparation between the other 2 groups to HG group. All the data are presented are expressed as means ± Std for 3 independent replicates and significant (*, $p<0.05$) difference comparing with HG are indicated

Figure 7. In-depth looipops figures analysis of RNA expression and DNA methylation of *Fgl2*(A,B), *Gulo*(C,D), *Kcnip*(E,F) and *Nmu*(G,H) within the HG/LG and TIIA/HG comparisons

Figure 8 Canonical pathways identified by IPA for all significant and reliable Differentially expressed genes in HG versus LG (A) and TIIA versus HG (B) from mes-13 cells after 5 days treatment. Canonical pathways are displayed as the –log(p-value) with the threshold of 1.3 indicating the minimum significance level. Length of the bars represents the significant associations.

Figure 9. The 10 most associated tox results related to HG versus LG (upper panel) and TIIA versus HG (lower panel) with the threshold of 1.3 (–log(p-value)) indicating the minimum significance level

Figure 10. The 10 most associated disease related to HG versus LG (upper panel) and TIIA versus HG (lower panel) with the threshold of 1.3 (–log(p-value)) indicating the minimum significance level

Table 1. Real-time q-PCR Primers information of validated genes of interest

Genes	Primer Sequence (5'-3')	Amplicon Size (bp)
Nmu	F: CTCAAAGATTGCAGCCAGAAC R: ATCACTATACGGCAAAGCTCC	87
Fgl2	F: AAGTGTTCCAAGTGTCCCAG R: TGCTGTTTCTGTGATCAGGG	101
Gulo	F: AAACTGGGCGAAGACCTATG R: GATGTCTGAAGGCGAGTGG	105
Kcnip2	F: GAGAGTTTGTCCGAATCCCG R: TCTCTGCGTGTGAACTTGG	106
β-actin	F: ACCTTCTACAATGAGCTGCG R: CTGGATGGCTACGTACATGG	106

Table 2 Top 50 annotated genes showing the highest log_2-fold change in either direction in high glucose treated group (HG) over low glucose treated group (LG), ranked by log_2-fold change

Increased (HG/LG)		Decreased (HG/LG)	
Symbol	Log2 fold change	Symbol	Log2 fold change
Nmu	4.129	*Zic2*	-4.626
Them5	3.959	*Gm14827*	-3.848
Dhh	3.766	*Lyz*	-3.848
Hsd3b1	3.659	*Nutm1*	-3.626
Cd300a	3.544	*Sh3bgr*	-3.626
Cyp2ab1	3.544	*Grin1*	-3.501
Fbxl13	3.544	*Gulo*	-3.041
Insyn2	3.544	*Kcnip2*	-3.041
Arhgap6	3.281	*Tssk2*	-3.041
C130021I20Rik	3.281	*C11orf98*	-2.848
C4A/C4B	3.281	*Hist2h2bf*	-2.848
Dpep2	3.281	*Il23r*	-2.848
E130102H24Rik	3.281	*Tnfrsf25*	-2.848
Entpd1	3.281	*Smyd1*	-2.742
Pbld	3.281	*Ankrd61*	-2.626
Pga5	3.281	*Aox4*	-2.626
Scn1a	3.281	*C11orf65*	-2.626
Snora5c	3.281	*Ephx4*	-2.626
Zfp345 (includes others)	3.281	*Fcer1g*	-2.626
Kcnj15	3.129	*Mir1191*	-2.626
Obscn	3.129	*Mir8091*	-2.626
Cd59a	2.959	*Npas3*	-2.626
Hnf4a	2.959	*Mamdc2*	-2.501
Acsm2a	2.766	*Myo7b*	-2.501
Ces2f	2.766	*Olfr99*	-2.501
Hpgds	2.766	*C19orf66*	-2.363
Islr2	2.766	*Gng8*	-2.363
Klk3	2.766	*Mesp2*	-2.363
Ldhd	2.766	*Slc4a5*	-2.363
Lipn	2.766	*Bmp8b*	-2.157
Mkln1os	2.766	*C1qtnf3*	-2.157
Nckap5	2.766	*Atp2a1*	-2.041
Kiaa1324	2.681	*Cd160*	-2.041
Akap5	2.544	*Ces1f*	-2.041
Cfap45	2.544	*Cyp4f12*	-2.041
Chn1os3	2.544	*Dusp13*	-2.041
Cyp2j5	2.544	*Epstil*	-2.041
Cyp4f22	2.544	*Gbp8*	-2.041
Fam19a5	2.544	*GJA4*	-2.041
Gpr132	2.544	*Mapk10*	-2.041
Icam1	2.544	*Mc1r*	-2.041
Pknox2	2.544	*Myo16*	-2.041
Rab39b	2.544	*Nrp*	-2.041

Slc22a6	2.544	*Serpinb9f (includes others)*	-2.041
Sox21	2.544	*Slc23a1*	-2.041
Tcp11	2.544	*Tmem266*	-2.041
Fgl2	2.418	*Tmod1*	-2.041
Gm19589	2.418	*Wfdc3*	-2.041
4930447K03Rik	2.281	*Ccdc116*	-1.967

Table 3 Top 50 annotated genes showing the highest log_2-fold change in either direction in 5μM TIIA treated group (TIIA) over HG, ranked by log_2-fold change

Increased (TIIA/HG)		Decreased (TIIA/HG)	
Symbol	Log_2 fold change	Symbol	Log_2 fold change
Gsta5	4.727	*Lcn2*	-4.756
Gsta1	4.523	*Ace2*	-4.586
Sh3bgr	3.999	*Gm19589*	-4.46
Ugt2b28	3.999	*Hspa12a*	-4.46
Il23r	3.906	*Iigp1*	-4.46
Htra3	3.806	*Steap4*	-4.393
Kchn4	3.806	*Ccdc33*	-4.323
Adam32	3.584	*Abca12*	-4.171
Snora2b	3.584	*Lpl*	-4.001
Ly6a (includes others)	3.321	*Them5*	-4.001
Lyz	3.321	*Trim30a/Trim30d*	-3.908
Msc	3.321	*MS4a10*	-3.808
Nostrin	3.321	*Dpt*	-3.701
Nyx	3.321	*S100g*	-3.701
Tnfrsf25	2.806	*Cd300a*	-3.586
Bmp8b	2.584	*Cyp4f22*	-3.586
Fcer1g	2.584	*Irf4*	-3.586
Itgb2l	2.584	*Ly6a (includes others)*	-3.586
Nkx6-3	2.584	*Nr1i3*	-3.586
Wscd2	2.584	*Tll1*	-3.586
Dusp13	2.458	*Ube2ql1*	-3.586
Rorc	2.458	*Nad+*	-3.481
Gm4432	2.414	*Cccdc160*	-3.46
Rapsn	2.368	*Gli2*	-3.323
Chrm1	2.321	*mir-761*	-3.323
Dpf3	2.321	*Obscn*	-3.171
Gja4	2.321	*Pla2r1*	-3.171
Mesp2	2.321	*Rcsd1*	-3.171
Mir1191	2.321	*3830432H09rik*	-3.001
Mpz	2.321	*A630001g21rik*	-3.001
Nalcn	2.321	*Snord19*	-3.001
Slc23a1	2.321	*Inmt*	-2.971
Slc4a5	2.321	*Ccl5*	-2.808
Snora43	2.321	*Histih2bi*	-2.808
Tssk2	2.321	*Phf24*	-2.808
Wfdc3	2.321	*Agt*	-2.645
Snora23	2.169	*Fermt1*	-2.586
Tfr2	2.169	*Galnt18*	-2.586
Ankrd61	2.114	*Gpr132*	-2.586
Ankrd63	1.999	*Il23a*	-2.586
Arsj	1.999	*Pde11a*	-2.586
Atp2a1	1.999	*Plxnc1*	-2.586
C11orf98	1.999	*Prdm1*	-2.586
C19orf66	1.999	*Rbp4*	-2.586

Ephx4	1.999	*Timd2*	-2.586
Gng8	1.999	*Ttyh1*	-2.586
Grin1	1.999	*Tulp2*	-2.586
Gulo	1.999	*Hist1h2al*	-2.504
Kcnip2	1.999	*Rsad2*	-2.475
Kl	1.999	*Kiaa1324*	-2.46

Table 4 Correlation of DNA promoter methylation ratio from SureSelect Methyl-seq and fold change of gene expression from RNA-seq for genes of interest

Genes of interest	DNA Promoter methylation ratio of HG/LG	DNA Promoter methylation ratio of TIIA/HG	Fold change of expression in HG/LG from RNA-seq	Fold change of expression in TIIA/HG from RNA-seq
Fgl2	-10.324	7.265	5.346	0.273
Gulo/(GLO)	18.530	-14.526	0.121	3.997
Kcnip2/KChIP2	11.567	-4.748	0.121	3.997
Nmu	-0.526	12.378	17.495	0.555

References

(1) Cooper, M. E. (1998) Pathogenesis, prevention, and treatment of diabetic nephropathy. *Lancet 352*, 213-219.

(2) Nguyen, D. V., Shaw, L. C., and Grant, M. B. (2012) Inflammation in the pathogenesis of microvascular complications in diabetes. *Front Endocrinol (Lausanne) 3*, 170.

(3) Sharma, D., Bhattacharya, P., Kalia, K., and Tiwari, V. (2017) Diabetic nephropathy: New insights into established therapeutic paradigms and novel molecular targets. *Diabetes Res Clin Pract 128*, 91-108.

(4) Abdo, S., Zhang, S. L., and Chan, J. S. (2015) Reactive Oxygen Species and Nuclear Factor Erythroid 2-Related Factor 2 Activation in Diabetic Nephropathy: A Hidden Target. *J Diabetes Metab 6*.

(5) Han, Y., Xu, X., Tang, C., Gao, P., Chen, X., Xiong, X., Yang, M., Yang, S., Zhu, X., Yuan, S., Liu, F., Xiao, L., Kanwar, Y. S., and Sun, L. (2018) Reactive oxygen species promote tubular injury in diabetic nephropathy: The role of the mitochondrial ros-txnip-nlrp3 biological axis. *Redox Biol 16*, 32-46.

(6) Fridlyand, L. E., and Philipson, L. H. (2005) Oxidative reactive species in cell injury: Mechanisms in diabetes mellitus and therapeutic approaches. *Ann N Y Acad Sci 1066*, 136-151.

(7) Kiritoshi, S., Nishikawa, T., Sonoda, K., Kukidome, D., Senokuchi, T., Matsuo, T., Matsumura, T., Tokunaga, H., Brownlee, M., and Araki, E. (2003) Reactive oxygen species from mitochondria induce cyclooxygenase-2 gene expression in human mesangial cells: potential role in diabetic nephropathy. *Diabetes 52*, 2570-2577.

(8) Koya, D., Hayashi, K., Kitada, M., Kashiwagi, A., Kikkawa, R., and Haneda, M. (2003) Effects of antioxidants in diabetes-induced oxidative stress in the glomeruli of diabetic rats. *J Am Soc Nephrol 14*, S250-253.

(9) Yamamoto, T., Nakamura, T., Noble, N. A., Ruoslahti, E., and Border, W. A. (1993) Expression of transforming growth factor beta is elevated in human and experimental diabetic nephropathy. *Proc Natl Acad Sci U S A 90*, 1814-1818.

(10) Bakin, A. V., Stourman, N. V., Sekhar, K. R., Rinehart, C., Yan, X., Meredith, M. J., Arteaga, C. L., and Freeman, M. L. (2005) Smad3-ATF3 signaling mediates TGF-beta suppression of genes encoding Phase II detoxifying proteins. *Free Radic Biol Med 38*, 375-387.

(11) Zhang, D. D. (2006) Mechanistic studies of the Nrf2-Keap1 signaling pathway. *Drug Metab Rev 38*, 769-789.

(12) Li, W., Guo, Y., Zhang, C., Wu, R., Yang, A. Y., Gaspar, J., and Kong, A. N. (2016) Dietary Phytochemicals and Cancer Chemoprevention: A Perspective on Oxidative Stress, Inflammation, and Epigenetics. *Chem Res Toxicol 29*, 2071-2095.

(13) Lee, J. H., Khor, T. O., Shu, L., Su, Z. Y., Fuentes, F., and Kong, A. N. (2013) Dietary phytochemicals and cancer prevention: Nrf2 signaling, epigenetics, and cell death mechanisms in blocking cancer initiation and progression. *Pharmacol Ther 137*, 153-171.

(14) Bahadoran, Z., Mirmiran, P., and Azizi, F. (2013) Potential efficacy of broccoli sprouts as a unique supplement for management of type 2 diabetes and its complications. *J Med Food 16*, 375-382.

(15) Jimenez-Osorio, A. S., Gonzalez-Reyes, S., and Pedraza-Chaverri, J. (2015) Natural Nrf2 activators in diabetes. *Clin Chim Acta 448*, 182-192.

(16) Zheng, H., Whitman, S. A., Wu, W., Wondrak, G. T., Wong, P. K., Fang, D., and Zhang, D. D. (2011) Therapeutic potential of Nrf2 activators in streptozotocin-induced diabetic nephropathy. *Diabetes 60*, 3055-3066.

(17) Xu, S., and Liu, P. (2013) Tanshinone II-A: new perspectives for old remedies. *Expert Opin Ther Pat 23*, 149-153.
(18) An, L., Peng, L. Y., Sun, N. Y., Yang, Y. L., Zhang, X. W., Li, B., Liu, B. L., Li, P., and Chen, J. (2018) Tanshinone IIA Activates Nuclear Factor-Erythroid 2-Related Factor 2 to Restrain Pulmonary Fibrosis via Regulation of Redox Homeostasis and Glutaminolysis. *Antioxid Redox Signal*.
(19) Wang, L., Zhang, C., Guo, Y., Su, Z. Y., Yang, Y., Shu, L., and Kong, A. N. (2014) Blocking of JB6 cell transformation by tanshinone IIA: epigenetic reactivation of Nrf2 antioxidative stress pathway. *AAPS J 16*, 1214-1225.
(20) Cai, M., Guo, Y., Wang, S., Wei, H., Sun, S., Zhao, G., and Dong, H. (2017) Tanshinone IIA Elicits Neuroprotective Effect Through Activating the Nuclear Factor Erythroid 2-Related Factor-Dependent Antioxidant Response. *Rejuvenation Res 20*, 286-297.
(21) Sui, H., Zhao, J., Zhou, L., Wen, H., Deng, W., Li, C., Ji, Q., Liu, X., Feng, Y., Chai, N., Zhang, Q., Cai, J., and Li, Q. (2017) Tanshinone IIA inhibits beta-catenin/VEGF-mediated angiogenesis by targeting TGF-beta1 in normoxic and HIF-1alpha in hypoxic microenvironments in human colorectal cancer. *Cancer Lett 403*, 86-97.
(22) Gao, H., Huang, L., Ding, F., Yang, K., Feng, Y., Tang, H., Xu, Q. M., Feng, J., and Yang, S. (2018) Simultaneous purification of dihydrotanshinone, tanshinone I, cryptotanshinone, and tanshinone IIA from Salvia miltiorrhiza and their anti-inflammatory activities investigation. *Sci Rep 8*, 8460.
(23) Liu, T., Jin, H., Sun, Q. R., Xu, J. H., and Hu, H. T. (2010) The neuroprotective effects of tanshinone IIA on beta-amyloid-induced toxicity in rat cortical neurons. *Neuropharmacology 59*, 595-604.
(24) Chen, X., Wu, R., Kong, Y., Yang, Y., Gao, Y., Sun, D., Liu, Q., Dai, D., Lu, Z., Wang, N., Ge, S., and Wang, F. (2017) Tanshinone IIA attenuates renal damage in STZ-induced diabetic rats via inhibiting oxidative stress and inflammation. *Oncotarget 8*, 31915-31922.
(25) Fan, K., Li, S., Liu, G., Yuan, H., Ma, L., and Lu, P. (2017) Tanshinone IIA inhibits high glucoseinduced proliferation, migration and vascularization of human retinal endothelial cells. *Mol Med Rep 16*, 9023-9028.
(26) Jiang, C., Zhu, W., Shao, Q., Yan, X., Jin, B., Zhang, M., and Xu, B. (2016) Tanshinone IIA Protects Against Folic Acid-Induced Acute Kidney Injury. *Am J Chin Med 44*, 737-753.
(27) Jiang, C., Zhu, W., Yan, X., Shao, Q., Xu, B., Zhang, M., and Gong, R. (2016) Rescue therapy with Tanshinone IIA hinders transition of acute kidney injury to chronic kidney disease via targeting GSK3beta. *Sci Rep 6*, 36698.
(28) Ahn, Y. M., Kim, S. K., Lee, S. H., Ahn, S. Y., Kang, S. W., Chung, J. H., Kim, S. D., and Lee, B. C. (2010) Renoprotective effect of Tanshinone IIA, an active component of Salvia miltiorrhiza, on rats with chronic kidney disease. *Phytother Res 24*, 1886-1892.
(29) Jiang, C., Shao, Q., Jin, B., Gong, R., Zhang, M., and Xu, B. (2015) Tanshinone IIA Attenuates Renal Fibrosis after Acute Kidney Injury in a Mouse Model through Inhibition of Fibrocytes Recruitment. *Biomed Res Int 2015*, 867140.
(30) Chen, G., Zhang, X., Li, C., Lin, Y., Meng, Y., and Tang, S. (2014) Role of the TGFbeta/p65 pathway in tanshinone A-treated HBZY1 cells. *Mol Med Rep 10*, 2471-2476.
(31) Kim, S. K., Jung, K. H., and Lee, B. C. (2009) Protective effect of Tanshinone IIA on the early stage of experimental diabetic nephropathy. *Biol Pharm Bull 32*, 220-224.
(32) Hadden, M. J., and Advani, A. (2018) Histone Deacetylase Inhibitors and Diabetic Kidney Disease. *Int J Mol Sci 19*.
(33) Keating, S. T., van Diepen, J. A., Riksen, N. P., and El-Osta, A. (2018) Epigenetics in diabetic nephropathy, immunity and metabolism. *Diabetologia 61*, 6-20.

(34) Leti, F., Morrison, E., and DiStefano, J. K. (2017) Long noncoding RNAs in the pathogenesis of diabetic kidney disease: implications for novel therapeutic strategies. *Per Med 14*, 271-278.
(35) Long, J., Badal, S. S., Ye, Z., Wang, Y., Ayanga, B. A., Galvan, D. L., Green, N. H., Chang, B. H., Overbeek, P. A., and Danesh, F. R. (2016) Long noncoding RNA Tug1 regulates mitochondrial bioenergetics in diabetic nephropathy. *J Clin Invest 126*, 4205-4218.
(36) Rubin, A., Salzberg, A. C., Imamura, Y., Grivitishvilli, A., and Tombran-Tink, J. (2016) Identification of novel targets of diabetic nephropathy and PEDF peptide treatment using RNA-seq. *BMC Genomics 17*, 936.
(37) Andrews, S. (2010) FastQC: a quality control tool for high throughput sequence data.
(38) Li, H., Handsaker, B., Wysoker, A., Fennell, T., Ruan, J., Homer, N., Marth, G., Abecasis, G., Durbin, R., and Genome Project Data Processing, S. (2009) The Sequence Alignment/Map format and SAMtools. *Bioinformatics 25*, 2078-2079.
(39) Kim, D., Langmead, B., and Salzberg, S. L. (2015) HISAT: a fast spliced aligner with low memory requirements. *Nat Methods 12*, 357-360.
(40) Krueger, F., and Andrews, S. R. (2011) Bismark: a flexible aligner and methylation caller for Bisulfite-Seq applications. *bioinformatics 27*, 1571-1572.
(41) Team, R. C. (2013) R: A language and environment for statistical computing.
(42) Wang, L., Feng, Z., Wang, X., Wang, X., and Zhang, X. (2010) DEGseq: an R package for identifying differentially expressed genes from RNA-seq data. *Bioinformatics 26*, 136-138.
(43) Storey, J. D. (2003) The positive false discovery rate: a Bayesian interpretation and the q-value. *The Annals of Statistics 31*, 2013-2035.
(44) Gaspar, J. M., and Hart, R. P. (2017) DMRfinder: efficiently identifying differentially methylated regions from MethylC-seq data. *BMC Bioinformatics 18*, 528.
(45) Yu, G., Wang, L. G., and He, Q. Y. (2015) ChIPseeker: an R/Bioconductor package for ChIP peak annotation, comparison and visualization. *Bioinformatics 31*, 2382-2383.
(46) Zhou, S., Treloar, A. E., and Lupien, M. (2016) Emergence of the Noncoding Cancer Genome: A Target of Genetic and Epigenetic Alterations. *Cancer Discov 6*, 1215-1229.
(47) Wenzel, S. E. (1997) Arachidonic acid metabolites: mediators of inflammation in asthma. *Pharmacotherapy 17*, 3S-12S.
(48) Peters-Golden, M., Canetti, C., Mancuso, P., and Coffey, M. J. (2005) Leukotrienes: underappreciated mediators of innate immune responses. *J Immunol 174*, 589-594.
(49) Smyth, E. M., and Fitzgerald, G. A. (2009) The eicosanoids: prostaglandins, thromboxanes, leukotrienes, and related compounds. *Basic and clinical pharmacology. 12th edition. McGraw Hill Medical*, 313-329.
(50) Smyth, E. M., Grosser, T., Wang, M., Yu, Y., and FitzGerald, G. A. (2009) Prostanoids in health and disease. *Journal of lipid research 50*, S423-S428.
(51) Makishima, M. (2005) Nuclear receptors as targets for drug development: regulation of cholesterol and bile acid metabolism by nuclear receptors. *Journal of pharmacological sciences 97*, 177-183.
(52) Burg, D., and Mulder, G. J. (2002) Glutathione conjugates and their synthetic derivatives as inhibitors of glutathione-dependent enzymes involved in cancer and drug resistance. *Drug metabolism reviews 34*, 821-863.
(53) Budhiraja, S., and Chugh, A. (2009) Neuromedin U: physiology, pharmacology and therapeutic potential. *Fundam Clin Pharmacol 23*, 149-157.
(54) Zhang, W., Sakoda, H., Miura, A., Shimizu, K., Mori, K., Miyazato, M., Takayama, K., Hayashi, Y., and Nakazato, M. (2017) Neuromedin U suppresses glucose-stimulated insulin secretion in pancreatic β cells. *Biochemical and biophysical research communications 493*, 677-683.

(55) Su, G., Liu, K., Wang, Y., Wang, J., Li, X., Li, W., Liao, Y., and Wang, Z. (2011) Fibrinogen-like protein 2 expression correlates with microthrombosis in rats with type 2 diabetic nephropathy. *J Biomed Res 25*, 120-127.

(56) Kashiba, M., Oka, J., Ichikawa, R., Kasahara, E., Inayama, T., Kageyama, A., Kageyama, H., Osaka, T., Umegaki, K., Matsumoto, A., Ishikawa, T., Nishikimi, M., Inoue, M., and Inoue, S. (2002) Impaired ascorbic acid metabolism in streptozotocin-induced diabetic rats. *Free Radic Biol Med 33*, 1221-1230.

(57) Sato, T., Kobayashi, T., Kuno, A., Miki, T., Tanno, M., Kouzu, H., Itoh, T., Ishikawa, S., Kojima, T., Miura, T., and Tohse, N. (2014) Type 2 diabetes induces subendocardium-predominant reduction in transient outward K+ current with downregulation of Kv4.2 and KChIP2. *Am J Physiol Heart Circ Physiol 306*, H1054-1065.

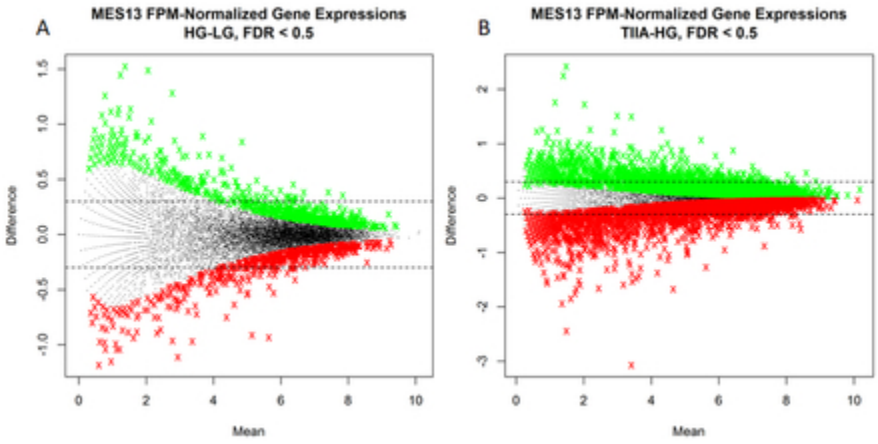

Figure 1. MA plots (log2 means vs. log2 difference) of the gene expressions in the two comparisons, HF vs. LG (A) and TIIA in HG vs. HG only (B). The two horizontal dotted lines correspond to log2 differences of +/- 0.3. The green or red symbols corresponds to upregulated or downregulated genes with FDR values of 0.5 or less

38x19mm (300 x 300 DPI)

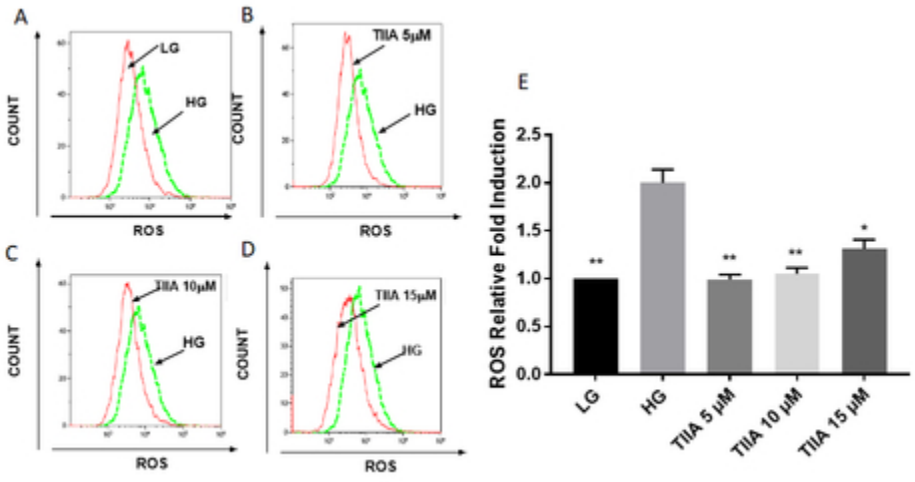

Figure 2. Effects of TIIA on production of intracellular reactive oxygen species (ROS) induced by 2 day treatment of high glucose (HG) In mouse kidney mes-13 cells via flow cytometry. Two days treatment of HG induced increase of intracellular ROS damage comparing with low glucose (LG) group(A), co-treatment of 5μM TIIA (B), 10 μM TIIA (C) and 15 μM TIIA(D) could protect mes-13 cells against ROS damage from HG. Relative ROS fold change normalized by LG (E) are expressed as means ± Std for 3 independent replicates and significant ($p<0.05$, *; $p<0.01$, **) difference comparing with HG are indicated.

39x22mm (300 x 300 DPI)

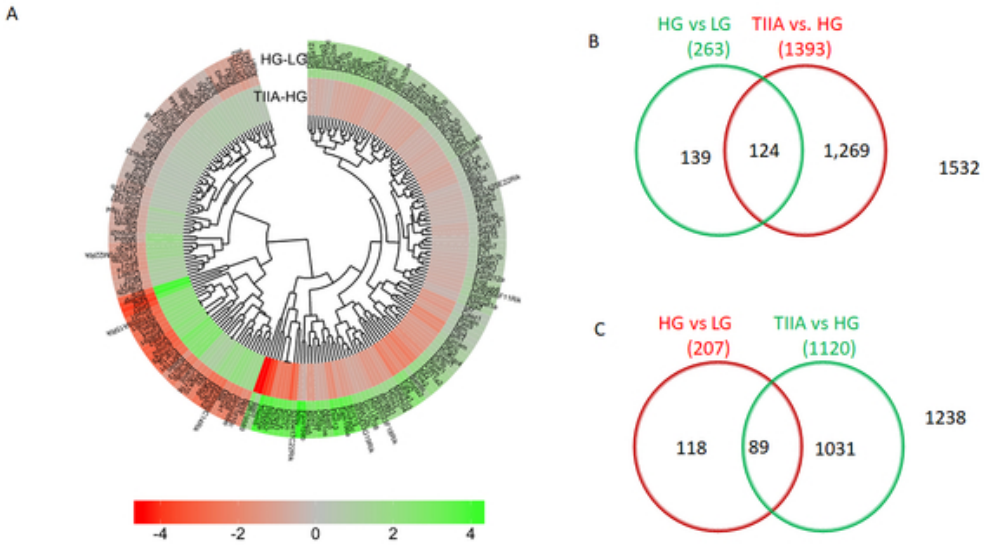

Figure 3. Overview of the differentially expressed genes in 2 comparisons among 3 groups (HG/LG and TIIA/HG). (A) Doughnut Heat map of 213 overlapped Genes with differential expression that appeared in HG versus LG group and TIIA versus HG group. (B, C) Venn diagrams comparing the up-regulated (green) and down-regulated genes (red) between HG versus LG group and TIIA versus HG group. Genes with log2 fold changes greater than 0.3 were counted.

24x13mm (600 x 600 DPI)

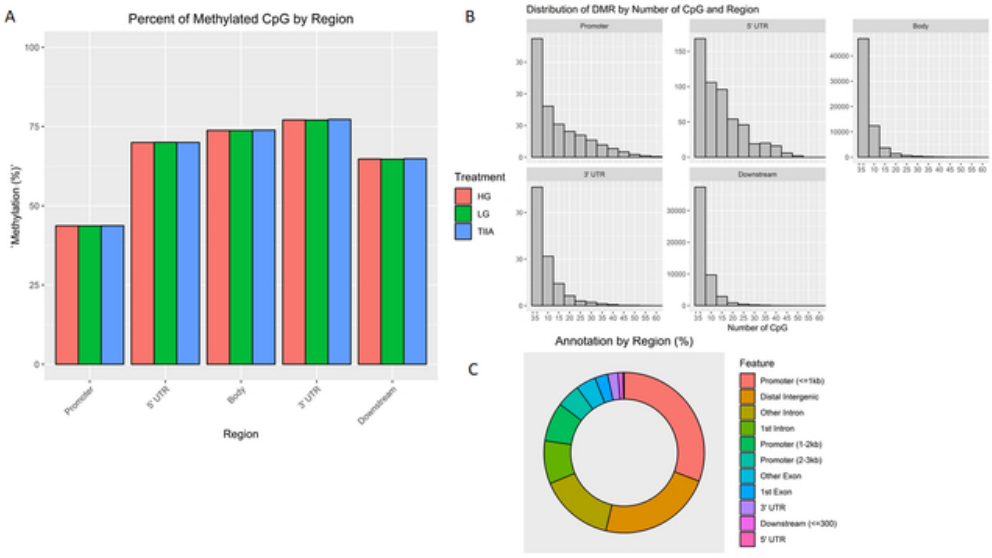

Figure 4. Sureselect Methyl-seq results (A) Percent of Methylated CpG by region and treatment; (B) Distribution of DMR by Number of CpG and Region; (C) DMR annotation by region (%)

27x16mm (600 x 600 DPI)

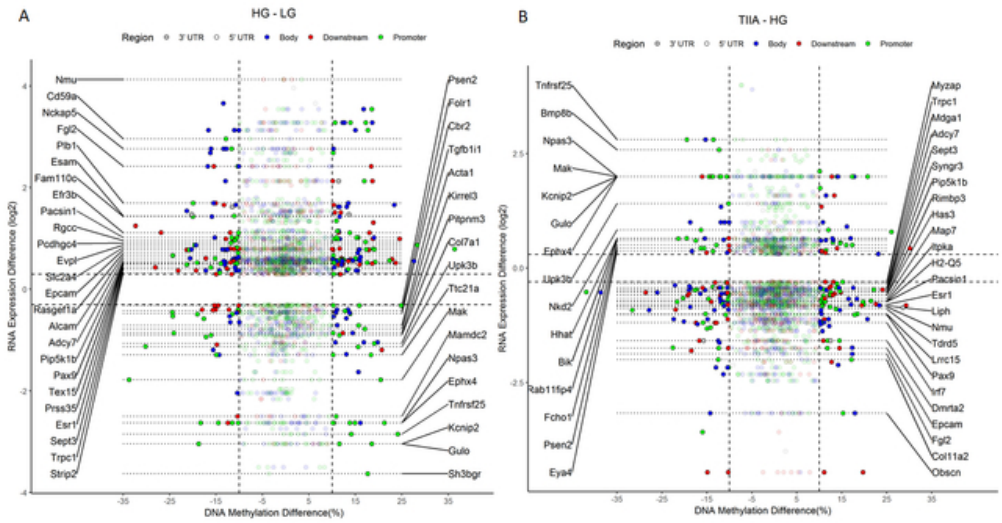

Figure 5. Starburst figures indicating correlation between RNA-seq and methyl-seq. The upper left and lower right quadrantal region of indicate those genes with reversed change of methylation and RNA expression in HG/LG (A) and TIIA/HG(B) comparisons

27x14mm (600 x 600 DPI)

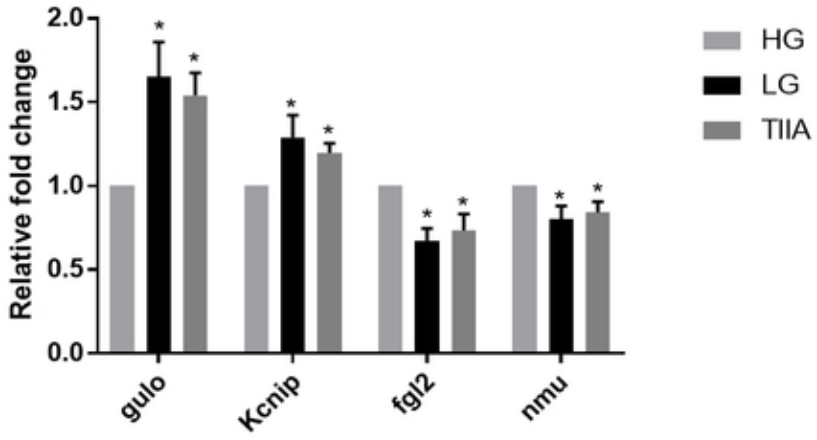

Figure 6. RNA qPCR validation for the genes of interest. The gene expressions from HG group were normalized to 1 and the relative fold changes were obtained from the comparation between the other 2 groups to HG group. All the data are presented are expressed as means ± Std for 3 independent replicates and significant (*, $p<0.05$) difference comparing with HG are indicated

44x28mm (300 x 300 DPI)

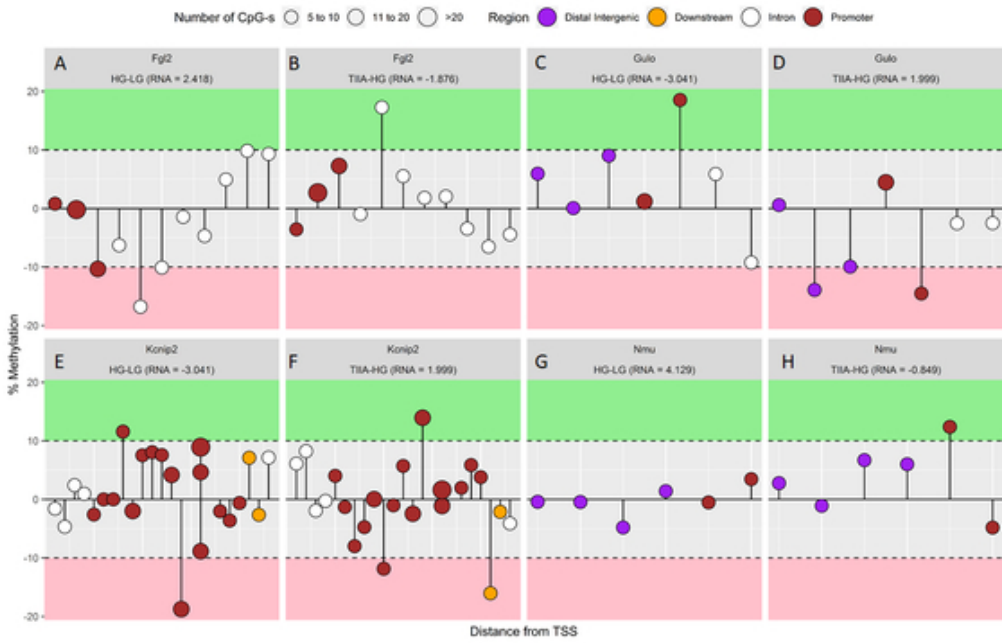

Figure 7. In-depth looipops figures analysis of RNA expression and DNA methylation of Fgl2(A,B), Gulo(C,D), Kcnip(E,F) and Nmu(G,H) within the HG/LG and TIIA/HG comparisons

23x15mm (600 x 600 DPI)

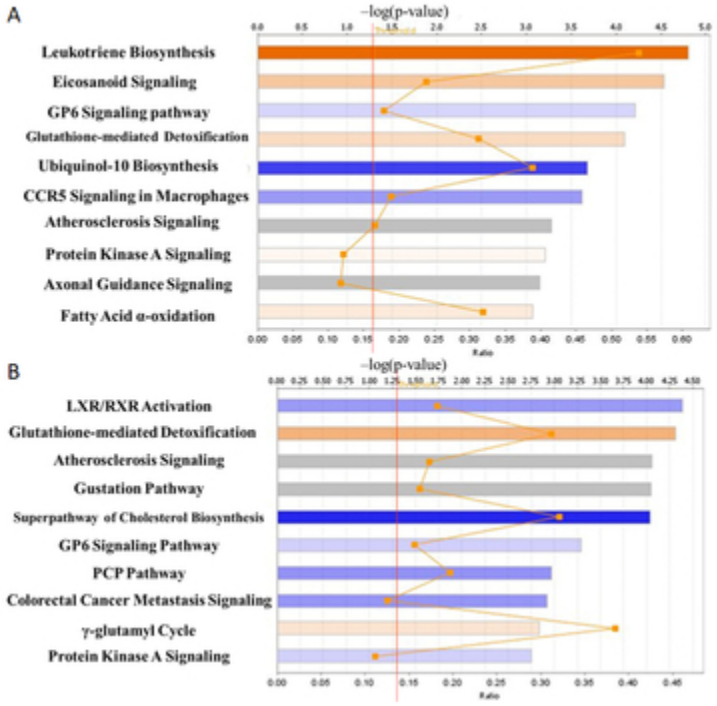

Figure 8. Canonical pathways identified by IPA for all significant and reliable Differentially expressed genes in HG versus LG (A) and TIIA versus HG (B) from mes-13 cells after 5 days treatment. Canonical pathways are displayed as the –log(p-value) with the threshold of 1.3 indicating the minimum significance level. Length of the bars represents the significant associations.

15x15mm (600 x 600 DPI)

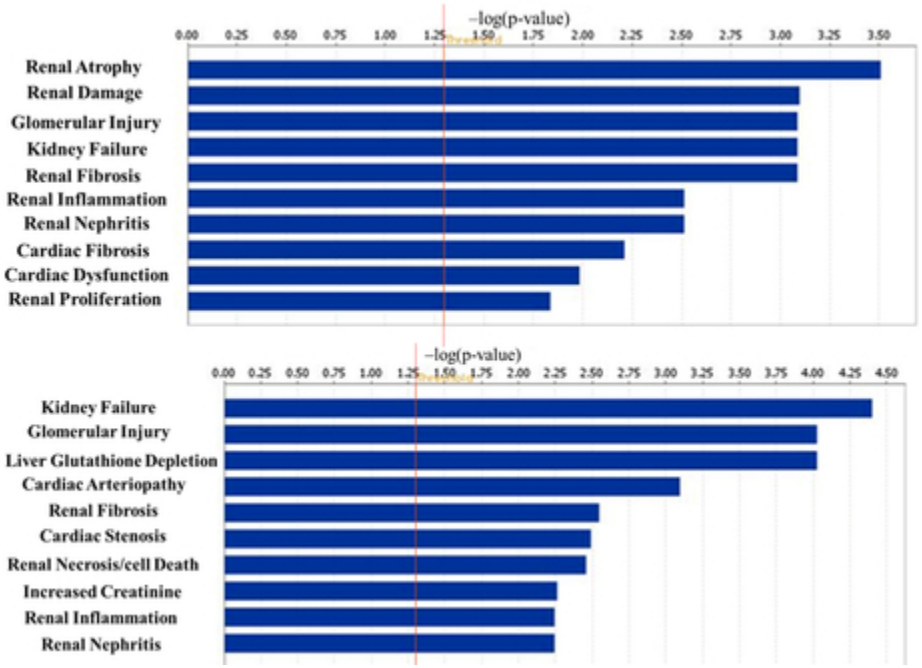

Figure 9. The 10 most associated tox results related to HG versus LG (upper panel) and TIIA versus HG (lower panel) with the threshold of 1.3 (−log(p-value)) indicating the minimum significance level

19x14mm (600 x 600 DPI)

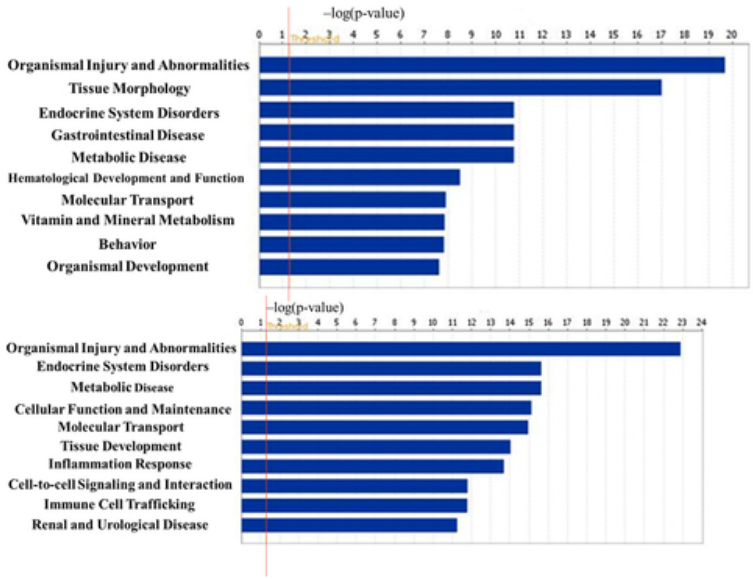

Figure 10. The 10 most associated disease related to HG versus LG (upper panel) and TIIA versus HG (lower panel) with the threshold of 1.3 (−log(p-value)) indicating the minimum significance level

27x16mm (600 x 600 DPI)